Warchola TJ, Flynn SL, Robbins LJ, Liu Y, Gauger T, Kovalchuk O, Alam MS, Wei S, Myers R, Bishop B, Lalonde SV, Gingras MK, Kappler A, Alessi DS, Konhauser KO.

Field- and Lab-Based Potentiometric Titrations of Microbial Mats from the Fairmont Hot Spring, Canada.

***Geomicrobiology Journal* 2017**

DOI: https://doi.org/10.1080/01490451.2017.1282557

Field- and Lab-Based Potentiometric Titrations of Microbial Mats from the Fairmont Hot Spring, Canada

Tyler J. Warchola[1], Shannon L. Flynn[1], Leslie J. Robbins[1], Yuxia Liu[1], Reed Myers[1], Tina Gauger[2], Olga Kovalchuk[1], Md. Samrat Alam[1], Siwen Wei[1], Stefan V. Lalonde[3], Andreas Kappler[2], Daniel S. Alessi[1], and Kurt O. Konhauser[1]

[1]Department of Earth and Atmospheric Sciences, University of Alberta, 1-26 Earth Sciences Building Edmonton, Alberta, Canada T6G 2E3
[2]Geomicrobiology Group, Center for Applied Geoscience, University of Tübingen, Sigwartstraβe 10, D-72076, Tübingen, Germany
[3]European Institute for Marine Studies, Technopôle Brest-Iroise, UMR 6538, Domaines Océaniques, Place Nicolas Copernic 29280, Plouzané, France

Abstract
Potentiometric titrations have been used as an effective means for determining surface reactivity and protonation constants for microbial surface ligands. The data gathered from the experiments have been applied to remediation projects with the aim of determining accurate metal immobilization estimates. These data have been generated in a laboratory setting using cultured microbes. We have attempted to investigate the implications of carrying out these titrations *in situ* at the sampling location, to attempt to determine reactivities more representative of the natural conditions. We hoped to distinguish the differences in titrating microbial mats in the field versus in the laboratory. Unfortunately, authigenic carbonate minerals complicated this process. We have highlighted the difficulties in titrating microbial mats in the field, and have made suggestions for future endeavors. It is clear that conditions under which surface reactivities are determined are much more complex in the field than in the laboratory. This preliminary study highlights the significant differences between field and laboratory surface reactivities, and the need for further *in situ* field investigations.

1.0 Introduction

Potentiometric titrations have been used to quantify the surface reactivity of microbes in controlled laboratory settings for nearly two decades (e.g., Fein et al., 1997; Fowle and Fein, 2000; Martinez et al., 2002; Borrok et al., 2004a). The use of potentiometric titrations and the development of surface complexation models (SCM) has many advantages over older empirical modeling approaches. Empirical models for adsorption include distribution coefficient, ion exchange, and the Langmuir and Freundlich isotherm which, as reviewed by Koretsky (2000), must be calibrated in the laboratory before being applied to a system of interest and cannot be extrapolated beyond strict experimental conditions. Surface complexation models, on the other hand, develop calculations that are applicable over a wide range of solution compositions and

conditions. The oversimplification of empirical K_d modeling was further emphasized by Bethke and Brady (2000), who found that optimistic rates of contaminant displacement from sediment surfaces by soil flushing or fresh recharge was predicted by K_d modelling, but not observed at remediation scale. Both studies pointed to the benefits of SCM, which we have chosen to use in this study.

Titration data provide information about the proton reactivity of the microbes, and when coupled to spectroscopic data, can be modeled to assess functional group variety and determine binding site concentrations on microbial surfaces and/or extracellular polymeric substances (EPS). The protonation constants (pKa) and site concentrations determined in these models can be coupled to metal adsorption experiments in order to determine the binding constants for the metals to each type of microbial surface functional groups (e.g., Fein et al., 2001; Phoenix et al., 2002). Much of this work has been undertaken with the goal of establishing a database of heavy metal – microbial binding constants that can be applied to predict metal immobilization efficiencies at specific bioremediation projects (Lovley and Coates, 1997; Malik, 2004).

A number of variables influence the efficiency of microbial cells and their extracellular exudates (e.g., EPS) to bind metals. These variables include, but are by no means limited to: pH, temperature, solution ionic strength, bacterial growth phase, surface area, mat morphology, nutrient availability, surface functional group blockage, organic acids, and the presence of *in situ* mineral phases (e.g., Fowle and Fein, 1999; Daughney et al., 2001; Yee and Fein, 2003; Lalonde et al, 2007a, b; Alessi and Fein, 2010). In natural systems these variables may fluctuate over short time scales. Environmental fluctuations not only impact instantaneous metal uptake by microbes, but can significantly alter growth conditions, and in turn, microbial surface characteristics. For this reason examining the impact of dynamic natural systems on the surface reactivity of microbes as determined by potentiometric titrations is of great interest. For example, Lalonde et al. (2007a) suggested that carbonate minerals closely associated, and inter-grown, with hot spring microbial mats in Yellowstone National Park account for the appearance of an inorganic ligand around pH 7 in excess charge curves. Borrok et al. (2004b) showed that bacteria thriving in contaminated environments exhibit significantly different adsorptive behavior compared to those from a previous study of uncontaminated environments (Borrok et al., 2004a). Given these considerations, a more realistic approach may be to employ potentiometric titrations in order to elucidate pKa's for use in metal surface complexation models (SCMs). SCMs are

capable of accounting for varied environmental conditions, and through a component additivity approach, may consider the impact of mineral phases associated with the mats on metal adsorption (Davis et al., 1998; Alessi and Fein, 2010).

Replicating environmental growth conditions and/or environmental fluctuations in a laboratory setting presents many practical obstacles. Potential changes in the reactivity of field samples during transport between the sampling site and laboratory could complicate replication. However, the extent of these changes and their effect on potentiometric titration results remains unconstrained. A simple solution to account for variability in field versus lab based titrations is to complete titrations *in situ* on site, thereby eliminating error associated with laboratory culturing and transport procedures, while simultaneously providing a more realistic assessment of microbial surface reactivity in the natural setting. Accordingly, the purpose of this study was to determine which differences, if any, exist in the results of field versus laboratory-based titrations. Furthermore, we seek to highlight the potential disparity in field conditions relative to laboratory cultures, and ultimately, to improve the application of quantitative metal adsorption predictions to more accurately replicate environmentally relevant conditions.

2. Study Area

The Fairmont Hot Springs Resort is built around a natural hot spring, and is located in the town of Fairmont Hot Springs in southeast British Columbia, Canada (Figure 1). The spring falls between the NW-SE trending Purcell and Redwall thrust faults, and is situated on the western slope of the Stanford Range (Pickering, 1954, Grasby & Hutcheon, 2001). Since 1912, a series of pools have been developed which are fed by spring water that passes through dolostone and diamictite layers (van Everdingen, 1972; Clague 1975). After being supplemented with chlorine, water from the pools is discharged on the south side of the main pool and over an embankment (approximately 6 meters in height) into Fairmont Creek which flows west and runs perpendicular to flow from the main pool discharge. The area between the embankment and the creek is characterized by a large (about 60 m^2) carbonate apron on which microbial mats are situated. It is from the apron that microbial mat samples for this study were collected. Figure 1 highlights the location of the Fairmont Hot Springs, the approximate location of our field laboratory, and the location of the sampling site.

The average annual air temperature ranges from a high of 24°C in July and August to a low of -16°C in January, and the average amount of precipitation ranges from 63.4 mm in June to 13.5 mm in February. During November, the month in which samples were collected, the average temperature ranges from 3°C to -7°C, with an average precipitation of 24.3 mm. These values are representative for the period between the years 2000 to 2012. On November 10th, 2014, when samples were collected, the air temperature ranged from -6°C to -16°C during sample extraction. There was light snow in the afternoon, accounting for 0.3 mm, 0.7 mm, and 0.3 mm of precipitation measured at 14:00, 17:00, and 20:00 hours, respectively. The atmospheric pressure at the site ranged from 1028 mb to 1038 mb (all weather and climate data from www.worldweatheronline.com).

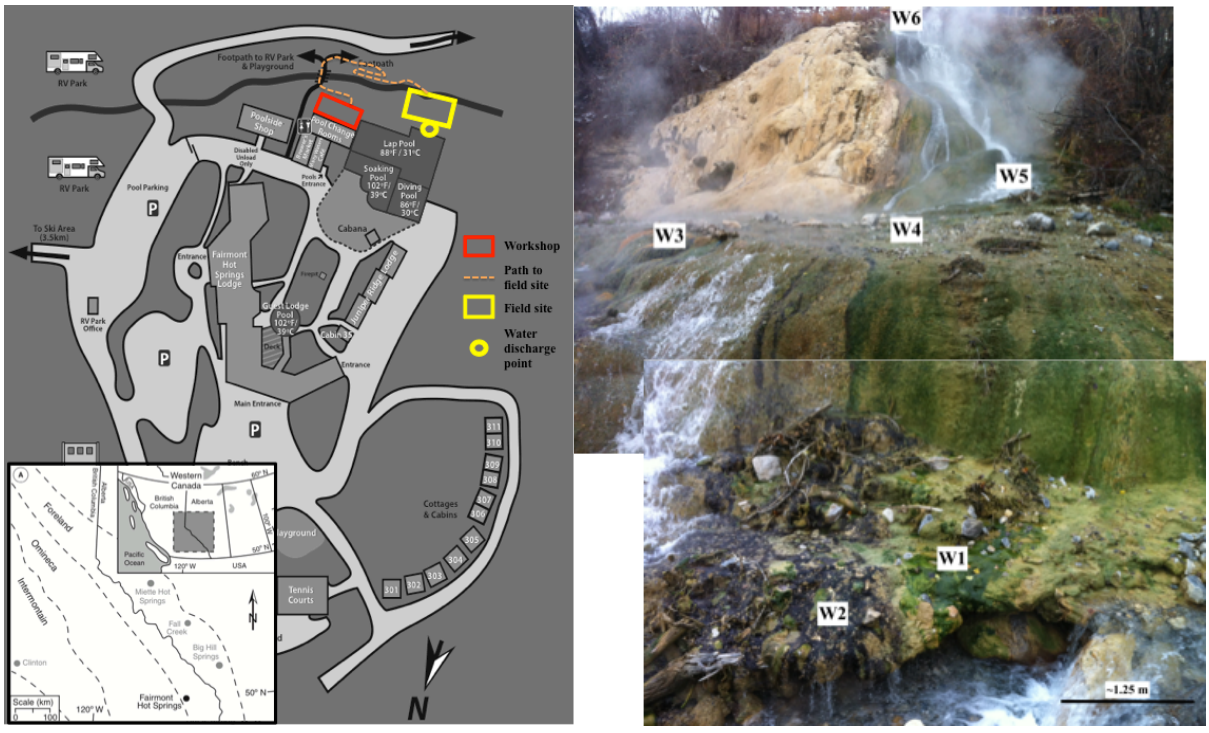

Figure 1. (A) The Fairmont Hot Springs location (inset) modified from Rainey and Jones (2009), and the layout of the resort. (B) Overview of the Fairmont field site with sampling locations labeled W1-W6; the horizontal distance across the mid-fan is approximately 15m. The image of the sampling site is the viewed standing on the south side of the yellow box (A), looking north.

3. Materials and Methods

3.1 *Sample collection from the field*

Water and microbial mat samples were collected from six separate locations along the carbonate apron described above. Ultimately, the discharging water crosses the apron and microbial mats, and flows into Fairmont Creek. Water temperature, pH, and conductivity measurements were taken at each of the six sites (labeled W1 through W6) using a multipurpose field meter (Accumet AP71, Fisher Scientific, Singapore).

Two 20 mL water samples were collected at each site, filtered through 0.22-micrometer nylon membranes into polypropylene tubes, and transported at 4˚C in order to measure cation and anion (NO_3-N, PO_4-P, Cl, SO_4-S) concentrations at the University of Alberta (UofA) Natural Resources Analytical Laboratory (NRAL). Water samples for cation analyses were acidified with five drops of trace metal grade nitric acid (16 M), while anion samples were not acidified. Analyses of anion concentrations for all water samples were performed using ion chromatography (Dionex Ion Chromatograph DX 600, Thermo Scientific, Sunnyvale, CA, USA) at the UofA within 36 h of sample collection, and values for NO_3^-, PO_4^{3-}, Cl^-, and SO_4^{2-} determined. Cation analyses were completed using Inductively Coupled Plasma – Mass Spectrometry (ICP-MS) at the Radiogenic Isotope Facility at the UofA, on an Elan 6100 Quadrupole ICP-MS.

Alkalinity of the water at each site was measured in the field and after 24 h at the UofA NRAL analytical facilities. For field measurements, a 50 mL polypropylene tube was filled with water at each site and immediately carried to our field laboratory (located <5 min walking distance from all sites, in a temporary space in the workshop at the Fairmont Hot Springs) for testing with a field alkalinity kit (Hach, Loveland, Colorado, USA). The 50 mL sample was transferred to a clean, 250 mL Erlenmeyer flask and diluted to 100 mL with 18.2 MΩ-cm ultrapure water. Bromcresol Green-Methyl Red indicator was dissolved in the water, after which the solution was titrated with 1.6 M sulfuric acid until a light pink color was achieved. Total alkalinity was calculated from the amount of acid added to the solution using standard conversion tables provided in the titration kit. To reduce the time between collection and analysis at the UofA, a second set of alkalinity samples were collected from the same locations on the morning of November 11, 2014 at 10:00 MST. Samples were transported and stored in a cooler, then submitted to the NRAL where they were tested within 24 h. Alkalinity was analyzed using a

SmartChem Discrete Wet Chemistry Analyzer (Model 200, Westco Scientific, Brookfield, CT, USA) and from these measurements CO_3^{2-} concentrations were subsequently calculated.

Four microbial mat samples, herein referred to as W1, W2, W3, and W4 (names correspond to sampling location of associated water), were collected from Fairmont Hot springs. Only water samples were collected at sites W5 and W6 (Figure 1). Carbonate grains were associated with all samples and could not be physically separated from the samples during the titrations conducted on site. Samples of each microbial mat were collected using a sterile, stainless steel spatula and stored in sterile 50 mL polypropylene tubes. Samples were transported back to the laboratory in a cooler at 4˚C, after which they were transferred to a dark 4˚C refrigerator. These mat samples were used in the comparative laboratory titration experiments, all of which were completed within one week of field sampling.

3.2 *Microscopy*

Field photographs, light microscope, scanning electron microscope (SEM) and transmission electron microscope (TEM) images of the samples are presented in Figure 2. For light microscopy, small amounts of wet, refrigerated sample were dissected with a sterile stainless steel scalpel, fixed to glass slides with several drops of low-fluorescence water-based fixative, air-dried for 15 min, and immediately examined. Photomicrographs were obtained using a Quorum Technologies 16 bit color QICAM and Zeiss Axioskop mot 2 microscope.

For SEM and TEM, cells were fixed in 2.5% gluteraldehyde-2% paraformaldehyde for four hours at 4^{o}C, and washed three times in 0.1 M phosphate buffer saline (PBS, pH 7.2). For TEM imaging, fixed samples were stained with 1% osmium tetroxide (OsO_4 in 0.12 M cacodylate buffer, pH 7.2) for 1 h, washed in 0.1 M PBS, and dehydrated through a graded ethanol series (15 min in each 50%, 70%, 90% and 100% solution). Dehydrated tissue was impregnated with low-viscosity Spurr resin and cured for 24 h at 80^{o}C. 60 nm-thick sections were cut using a Reichert-Jung ultramicrotome, mounted onto formvar and carbon-coated, 200-mesh, copper grids, and stained with a 2% uranyl acetate solution. A Philips FEI Morgagni 268 TEM (operating at 80 kV) was used to image the samples. For SEM imaging, cells were fixed and dehydrated as described above. Dehydrated cells were prepared by drying in a desiccation chamber overnight, placed on aluminum SEM stubs, sputter coated with gold, and imaged on a Philips FEI XL30 SEM operating at 20 kV.

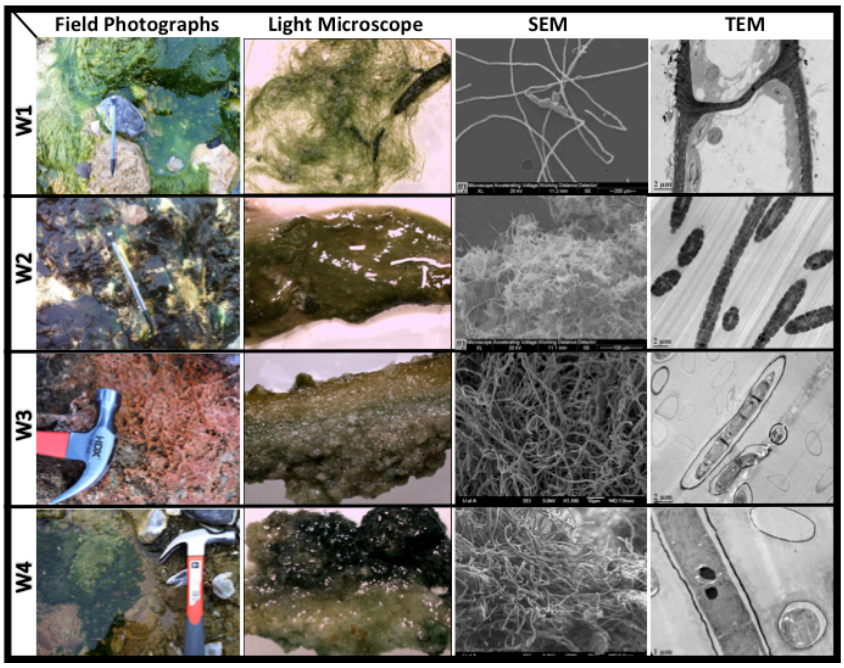

Figure 2. Images of mats at sites W1-W4.

3.3 *Sample preparation and acid-base titration*

All plastic and glassware used for solution preparation and potentiometric titrations were soaked in 10% nitric acid for 24 h and subsequently in sterile 18.2 MΩ-cm water for 48 h, before being rinsed three times with 18.2 MΩ-cm water and allowed to air-dry while inverted. Microbial mat samples were divided by weight into two groups for separate preparation and titration. One half of the sample material was prepared by one rinse (10 s agitation and 10 min soak), and then a harvest cycle (centrifugation for 10 min at 8,000 g) using 35 mL of 0.01 M $NaNO_3$ titration electrolyte. These samples are referred to herein as "electrolyte-wash samples". The second half was prepared by three alternating rinse (10 s agitation and 10 min soak) and harvest (centrifugation for 10 min at 8,000 g) cycles, using 35 mL 0.01 M EDTA for each rinse, followed by a fourth and final rinse using 0.01 M $NaNO_3$ electrolyte. The EDTA was used to simultaneously strip metals from the surface of the bacteria and bind metals in solution in order to make them unavailable for surface completion with the microbial surface ligands. Thus, the ligands were either protonated or deprotonated with no inferred interferences by metals in solution. This EDTA-wash procedure is intended to reveal the proton-binding behavior of the organic components comprising the biomass surface in a manner analogous to previous bacterial acid-base titrations. These samples are thus referred to as "EDTA-wash samples". The rinsing

solutions were passed through 0.45µm nylon filters and were subsequently analyzed for selected aqueous species. Our intention in titrating both $NaNO_3$- and EDTA-washed samples was to replicate the procedure of past studies in which the natural surface reactivity of samples in an aqueous solution containing metals ($NaNO_3$ wash) was compared with a completely metal-stripped microbial surface (EDTA wash). Unfortunately, the presence of carbonate influenced both sets of titrations, the implications of which will be discussed later.

For each titration, 0.4-0.5 g of prepared microbial mat sample (wet weight) was added to approximately 40 mL (precisely weighed) of electrolyte solution (0.01 M $NaNO_3$) and acidified with 2 M HCl to a pH of approximately 3.0. A double-junction glass pH electrode (Orion ROSS ultra, filled with 3 M KCl) was calibrated using commercial pH buffers (Thermo Fisher Scientific; pH 2.0, 3.0, 4.0, 7.0, 10.0). The pH electrode was mounted in flasks containing the prepared alkalimetric titration solutions along with a magnetic stir bar, titrant dispenser, thermocouple and nitrogen (N_2) gas line with a diffusion stone bubble. Solutions were sealed with Parafilm and purged with N_2 for 30 min prior to, and throughout titrations, to maintain a CO_2-free atmosphere in the flask. Titrations were carried out a minimum of three times. Blank titrations were performed for machine calibration, using bacteria-free 0.01 M $NaNO_3$.

Titrations were performed alkalimetrically from pH 3 to 11 using a Man-Tech Associated QC-Titrate autotitrator which variably delivered CO_2-free 0.01 M NaOH in 0.1 mL increments, with an average equilibration time between additions of 30 s. The volume of base added, and corresponding pH changes, were recorded at each titration step. Each addition of base occurred only after a pH electrode stability of 0.1 $mV \cdot s^{-1}$ was attained for a typical total titration time of 50 min. Once a pH of approximately 11 was achieved, reverse 'down-pH' titrations were performed, decreasing the suspension to pH 3 with aliquots of 0.01 M HCl in order to test the reversibility of proton binding on the cells. Due to time constraints, only forward-titrations were completed in the field, while both forward- and reverse-titrations were completed in the laboratory following transportation. Immediately following titrations, biomass was filtered onto pre-weighed 0.45µm filters and oven dried at 65^{o}C for 48 h for dry weight determination. As a proxy for cell integrity, pigment autofluorescence was examined for selected samples immediately pre- and post-titration. No change in the frequency or intensity of cell autofluorescence was observed.

To determine the acidity constants and concentrations of proton active functional groups on the bacterial surface, a non-electrostatic surface complexation model was chosen to fit the potentiometric titration data using linear programming (see Lalonde et al., 2008a,b; Lalonde et al., 2010), implemented in MATLAB (Mathworks, Natick, MA) to optimize ligand densities at points in a fixed pK_a interval (in this case, 4 to 10 in 0.2 increments). Furthermore, a least-squares optimization implemented in FITEQL 4.0 (Herbelin and Westall, 1999) was utilized to resolve acidity constants (expressed as pK_a, equivalent to $-\log K_a$) and ligand densities for a predetermined number of ligands. This permits the best description of the excess charge data. The charge balance in each titration step was calculated by the following charge balance equation:

$$[C_a - C_b] = [-Q] + [H^+] - [OH^-] \qquad (1)$$

Where $[C_a - C_b]$ is the concentration of acid added minus the concentration of base added; $[H^+]$ and $[OH^-]$ are the concentrations of proton and hydroxyl ions, respectively; and [-Q] is the negative charge excess owing to deprotonation of bacterial ligands in solution, normalized per gram of biomass.

A similar titration was conducted for a mixture of 0.01 M $NaNO_3$ background electrolyte solution and a powdered sample of carbonate that was isolated from the microbial mats. This titration served to represent the carbonate end-member of the system, i.e., to quantify the consumption of protons by carbonate mineral dissolution that would be interpreted as apparent surface reactivity in potentiometric titrations of the full mat samples. The initial mixture of approximately 3.5 g of carbonate and 40 mL of $NaNO_3$ was acidified to pH 3 using 1 mL of 12 M HCl. Upon addition of the concentrated HCl, $CO_{2(g)}$ formed and escaped the system. The solution was bubbled with Ar gas and stirred over the course of the titration to maintain a CO_2 free atmosphere. The high buffering capacity of carbonate necessitated the use of 0.1 M NaOH as the titrant, opposed to the other titrations in which 0.01 M NaOH was used. The results of this titration were used to assess the impact of carbonate on the interpreted surface reactivity of microbial mats.

4. Results

4.1 *Sample descriptions from the field*

Sampling sites were chosen to best represent conditions along a transect (from site W6-W1) following the flow of hot spring water from the discharge point to the creek. This provided aqueous chemistry and geochemical conditions across the carbonate apron. Different distances along this transect also promoted the growth of different types of microbial mats. In general, both water temperature and alkalinity decreased along the transect.

Site W1 was covered in a microbial mat composed of segmented, dark green filaments visible to the naked eye. Microbes in this mat are almost an order of magnitude larger in width than in the other three samples (~15 μm), and the filaments are much longer. Fine carbonate grains coat each filament as visible in the SEM images (Figure 2). The temperature of the water surrounding the mat was 18˚C, the pH 7.95, and the conductivity -4.4 mV. Alkalinity was tested in field and in the lab; the field alkalinity was 298 mg/L while the lab alkalinity was 207 mg/L. Anion analyses revealed the following concentrations: NO_3-N 0.05 mg/L, Cl 29.74 mg/L, and SO_4-S 224.1 mg/L. For all field sites, the concentration of major cations present (>0.1 ppm) can be viewed in Table 1.

Site W2 had a thin, opaque, blackish-purple, "gelatinous" microbial mat. Numerous microbes in this sample are morphologically similar to Cymbellales diatoms, approximately 5 μm in width and 18 μm in length. A long, segmented, filamentous bacterium with a width of about 1.8 μm is equally prevalent. Smaller (5μm in length and 0.1μm in width) spirochete-shaped bacteria are also occasionally observed on the surface of calcite grains. The water temperature around the mat was 27˚C, the pH 8.02, and the conductivity -9.3 mV. Field and lab alkalinity measurements were 380 mg/L and 403 mg/L, respectively. Anion analyses revealed the following concentrations: NO_3 0.09 mg/L, Cl 26.12 mg/L, and SO_4 233.7 mg/L.

Site W3 was covered in an orange, spongy, microbial mat. The mat is dominated by a filamentous, non-segmented bacterium, ~1 μm in width, and coated in fine (0.01 to 1 μm scale) carbonate grains (Figure 2). The filaments are also more irregular/contorted than the other samples, and exhibit sharper curves and more dramatic angles. The bacteria appear to be more densely packed, making the mat more cohesive than the previous two samples. When placed under anoxic conditions during titrations, the mat turned from orange to green. In general, the mat inhabited a subaerial environment where water flowed around the edges of the mat, as

opposed to the other mats that were continuously submerged. The temperature of the water flowing proximal to the mat was 27.6˚C, the pH was 7.9, and the conductivity was -2.2 mV. Field and lab alkalinity measurements were 185.2 mg/L and 254 mg/L, respectively. Anion analyses indicated concentrations of NO_3 0.12 mg/L, Cl 33.71 mg/L, and SO_4 239.3 mg/L.

Site W4 is characterized by a less extensive, but thicker and more compact green mat, whose filaments were less well defined than those of W1. Segmented, filamentous bacteria (~2μm in width) coated in carbonate dominated this mat (Figure 2). The filaments curved more smoothly than the sample collected at site W3, and fewer macroscopic pores were visible. Unlike the mat at site W1, this mat could be peeled easily from its substratum while maintaining its form. This mat inhabited a depression in the carbonate apron, which caused the overlying water column to be deeper and the flow rate of water to drop. The temperature and pH of the overlying water were 23.5˚C and 7.94, respectively, while the conductivity was -4.7 mV. Field and lab alkalinity measurements were 390.8 mg/L and 394 mg/L, respectively. Anions were present in concentrations of NO_3 0.11 mg/L, Cl 27.32 mg/L, and SO_4 235.0 mg/L.

No microbial mats were collected from sites W5 and W6, but water characteristics were measured. Site W5 is located at the base of a steep carbonate apron over which a waterfall forms as water leaves the commercial hot spring and makes its way to the creek below. The temperature of the water was 25.6˚C, pH was 7.81, and the conductivity was 3.7 mV. Field and laboratory alkalinity measurements were 399.6 mg/L and 269 mg/L, respectively. Anion analyses for W5 shows concentrations of NO_3 (0.12 mg/L), Cl (26.52 mg/L), and SO_4 (228.6 mg/L) at similar levels as the other sites.

Site W6 is located at the top of the carbonate apron, where the hot spring water enters the site from the commercial pool by means of man-made pipes. The water temperate and pH measured were 31.0˚C and 6.44, respectively, and the conductivity was 76.8 mV. Field and lab alkalinity measurements were 402.8 mg/L and 282 mg/L. Concentration for anions indicate levels of: NO_3 0.12 mg/L, Cl 28.05 mg/L, and SO_4 229.3 mg/L.

Analyte	**Na**	**Mg**	**Si**	**K**	**Ca**	**Sr**
Detection Limits (DL)	0.0005	0.002	0.005	0.006	0.031	0.00003
Units	**ppm**	**ppm**	**Ppm**	**Ppm**	**ppm**	**ppm**
F1-W1	16.7	69.2	9.47	3.45	220	2.02
F1-W2	17.0	70.9	9.66	3.53	248	2.13
F1-W3	16.6	69.4	9.48	3.42	249	2.11
F1-W4	16.9	70.1	9.48	3.51	245	2.10
F1-W5	17.6	73.1	9.80	3.66	260	2.13
F1-W6	16.9	70.6	9.51	3.45	252	2.09

Table 1. Cation concentrations (ppm) in hot spring water at each location.

4.2 *Field alkalinity*

From the alkalinity profile (Figure 3), spring water collected from the source (W6) has the highest alkalinity of 403 mg/L. The alkalinity concentrations decrease further from the source, which is the expected result when considering CO_2 degassing coupled to calcium carbonate ($CaCO_3$) precipitation. Water at W3 shows the most dramatic decline in alkalinity (as $CaCO_3$ (mg/L)). This sample was collected from a stagnant pool where carbonate precipitation is assumed to be ongoing.

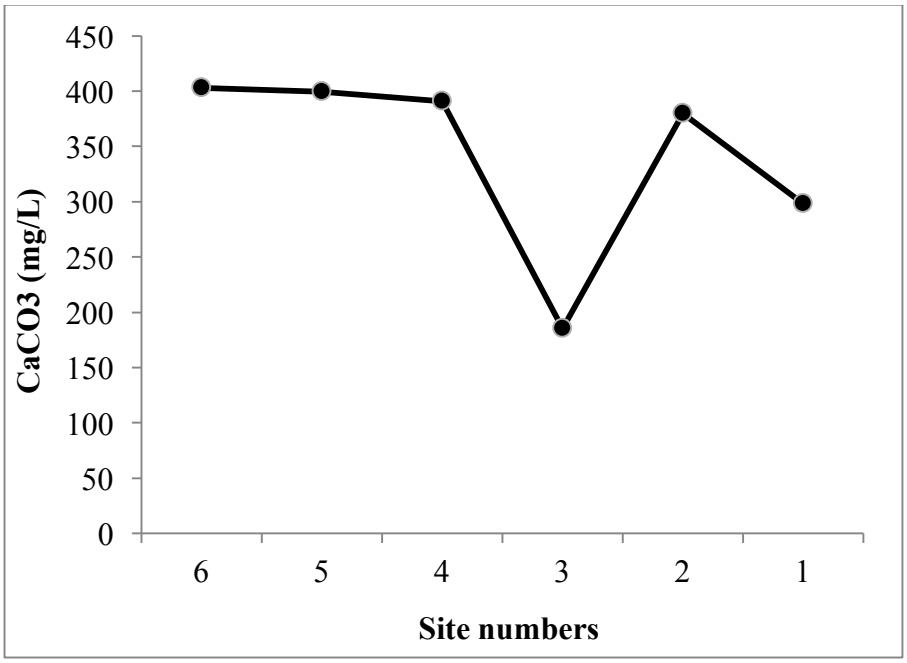

Figure 3. Alkalinity profile along carbonate fan. See Figure 1 for locations of sites along the carbonate apron, and relative distance from the commercial hot spring pool water discharge pipe.

4.3 *Potentiometric titrations*

Microbial mats were take from fields sites W1-W4, and transported approximately 5 minutes walking distance to a makeshift "titration shack" where titrations were immediately completed. Although the mats were not directly *in situ* during titration, we believe that the error induced by a <5 min transport from the sampling site to our field laboratory is negligible and warranted as being considered *in situ* given the generally long transport times (on the order of days) from field sites to laboratories. Titrations conducted *in situ* in an open hot spring system would also be impossible, as the flowing water would carry any acid added away from the titration site. The transport to the field laboratory is as close to "*in situ"* as these studies can be.

Only forward-titrations from pH 3-10 were completed on mats W1-W4 in the field due to time limitations, while both forward- and reverse-titrations were completed in the lab (Figure 4). While no difference is observed within the excess charge curves for the laboratory and field titrations of the separate mats, significant differences between the field and laboratory based titrations of the same mat samples are readily apparent, especially above pH 6. Generally, the field titrations show a rapid increase in excess charge (or low buffering capacity) between pH 8 and 9, except for the $NaNO_3$ washed samples at locations W1 and W4. The increase in excess charge is generally present at lower pH values in the lab titrations.

The pKa site concentration bar charts reinforce the inconsistency in the excess charge curves. For locations W3 and W4, field titrations indicate relatively high proton-active site concentrations around pH 10 (Figure 5). These sites are not detected at sampling locations W1 and W2, and they appear to be eliminated after transport to the laboratory. Additionally, EDTA washed samples tend to show higher site concentration, although the site concentrations between field and laboratory titrations differ depending on the sample titrated and show no coherent pattern.

Mat samples from all field locations show a marked increase in buffering capacity and excess charge around pH 9-10 (Figure 6). The buffering capacities of field titrations appear much less uniform than the lab titrations. An end-member carbonate titration produces a sinusoidal shaped buffering capacity line (Figure 7). The shape of the buffering capacity curve at site 2 appears to mimic the shape of this carbonate end-member. It is likely that portions of the

carbonate end-member buffering capacity curve are present at all sites, but to a lesser extent than at site W2 (Figure 6).

Forward and reverse titrations show hysteresis (Figure 8), which suggests the system is not in equilibrium during titration, and that either deprotonation during the up titration is not fully reversible or we are losing protons to carbonate dissolution and the evolution of $CO_{2(g)}$. Indeed, we are applying an equilibrium technique to a non-equilibrium system, so hysteresis is expected. Site 1 up and then down titration is closer than the other sites, in which down and then up titrations were performed. Overall, the data point to the impact of carbonates, inextricably bound into the mat matrix, that consume protons during potentiometric titrations. However, differences in laboratory and field titration experiments on systems containing identical quantities of biomass and carbonate precipitates show that mats collected in natural settings and titrated immediately have quite different surface reactivity than those stored for a period of days and then titrated. Thus, even conventional preservation techniques, such as storing mat samples on ice and then titrating in laboratories some days later, may inadequately characterize the actual in-situ surface reactivity of naturally-occurring microbial mats.

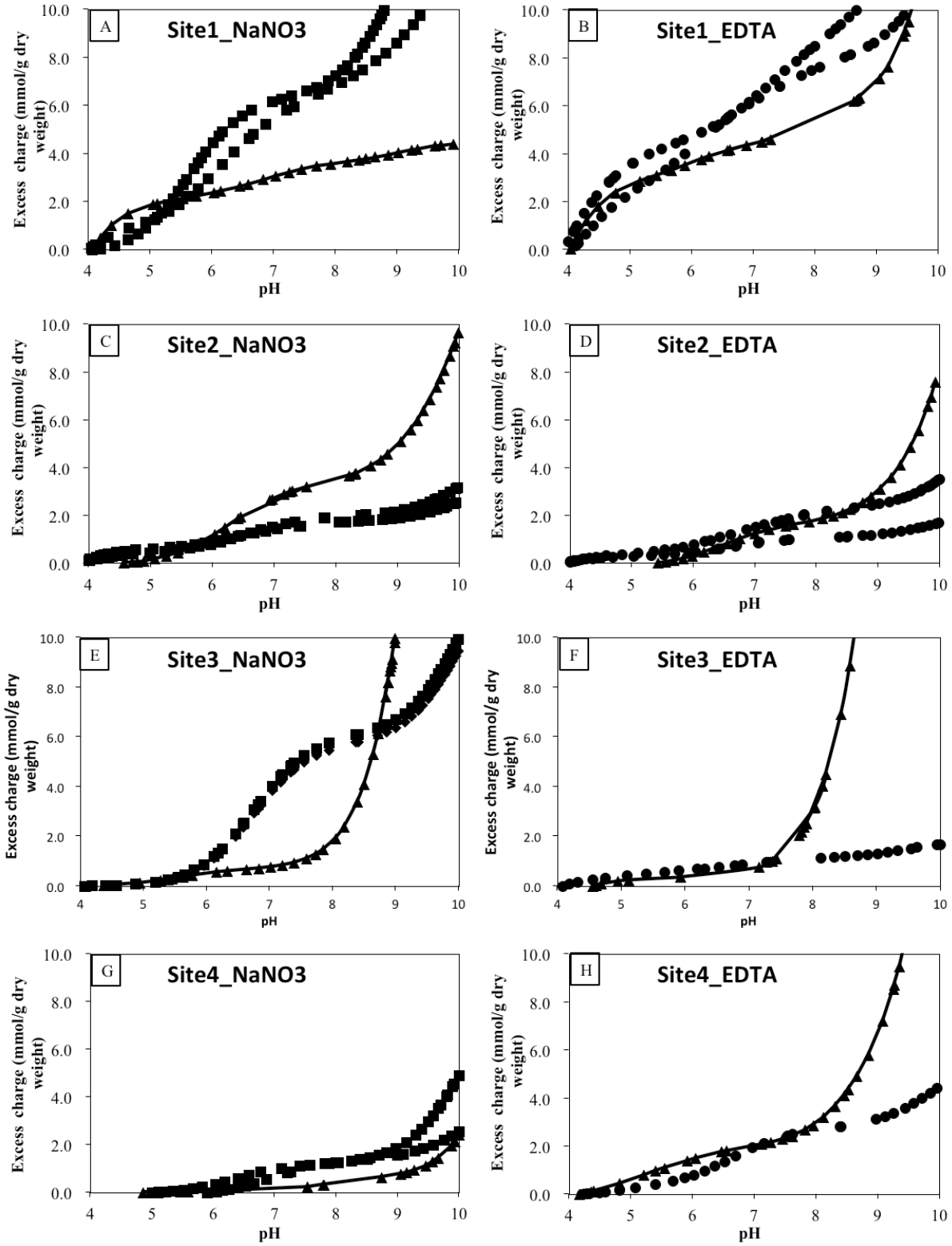

Figure 4. Titration data. Excess charge (y- axis) versus pH (x- axis). Squares and circles represent laboratory titrations for electrolyte-washed, and EDTA-washed samples, respectively. Triangles represent field titrations. Sites 1-4 refer to mats W1-W4.

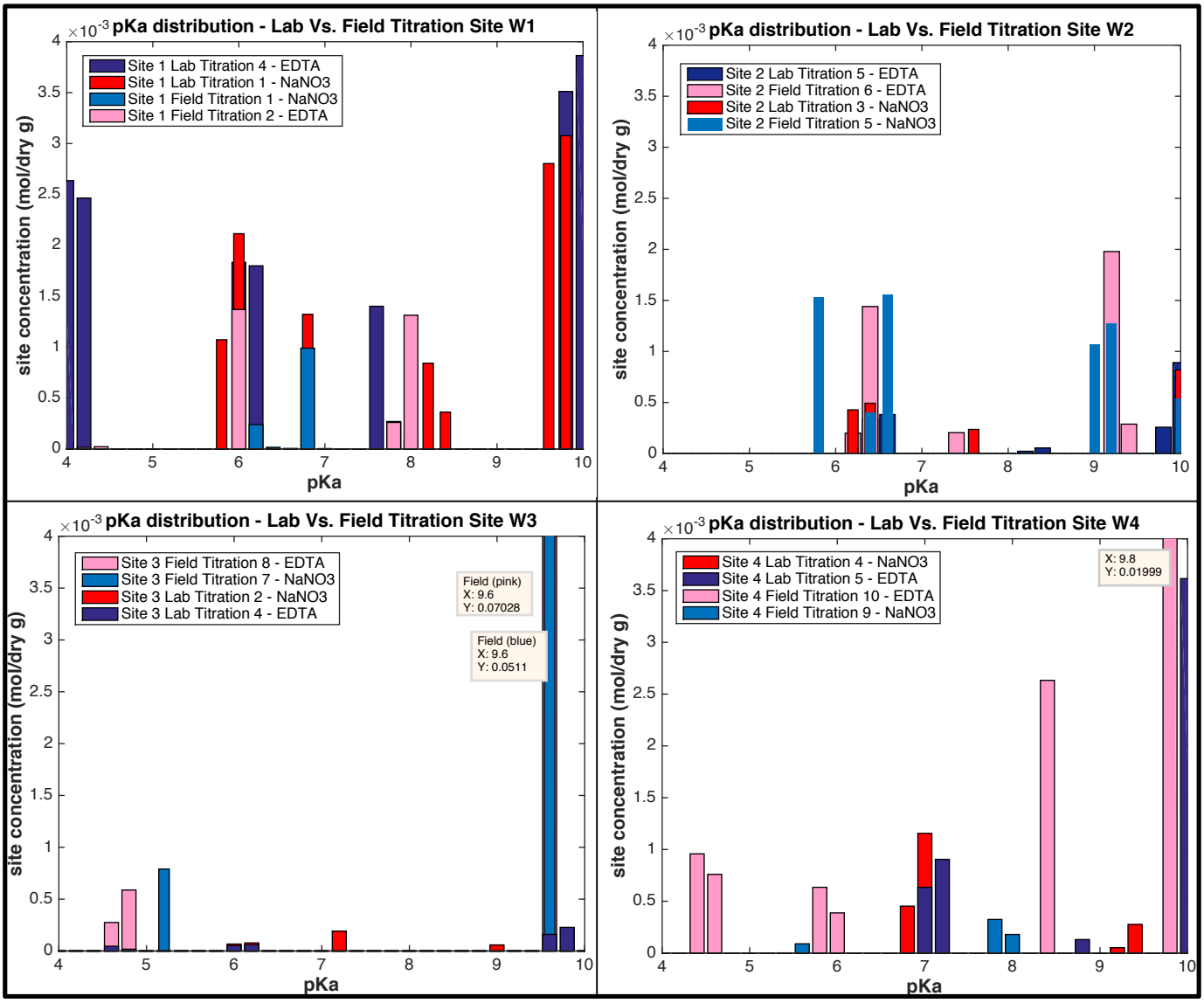

Figure 5. Modeled site concentrations between pKa 4 and 10.

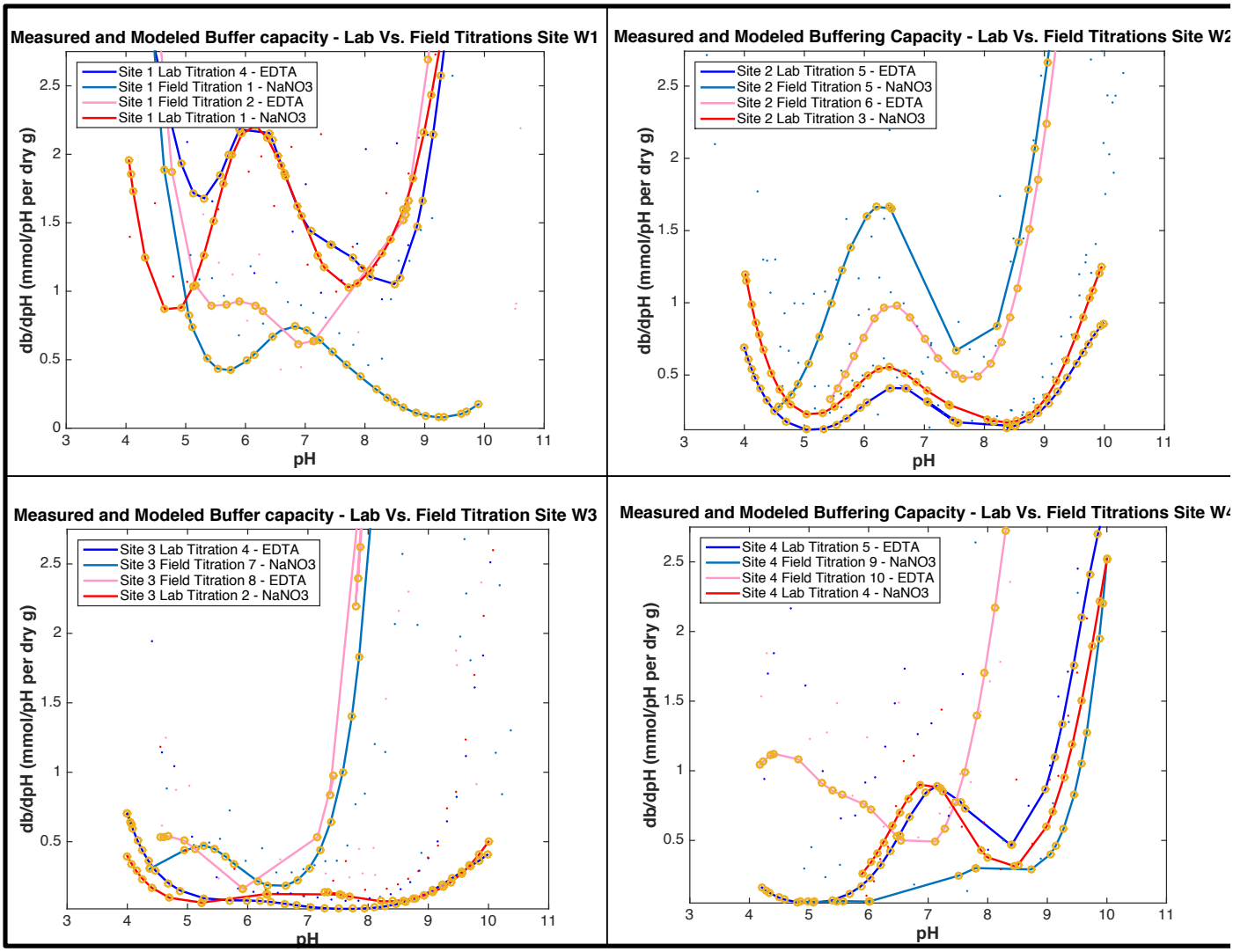

Figure 6. Modeled buffering capacity for lab and field titrations of samples from sites 1 to 4.

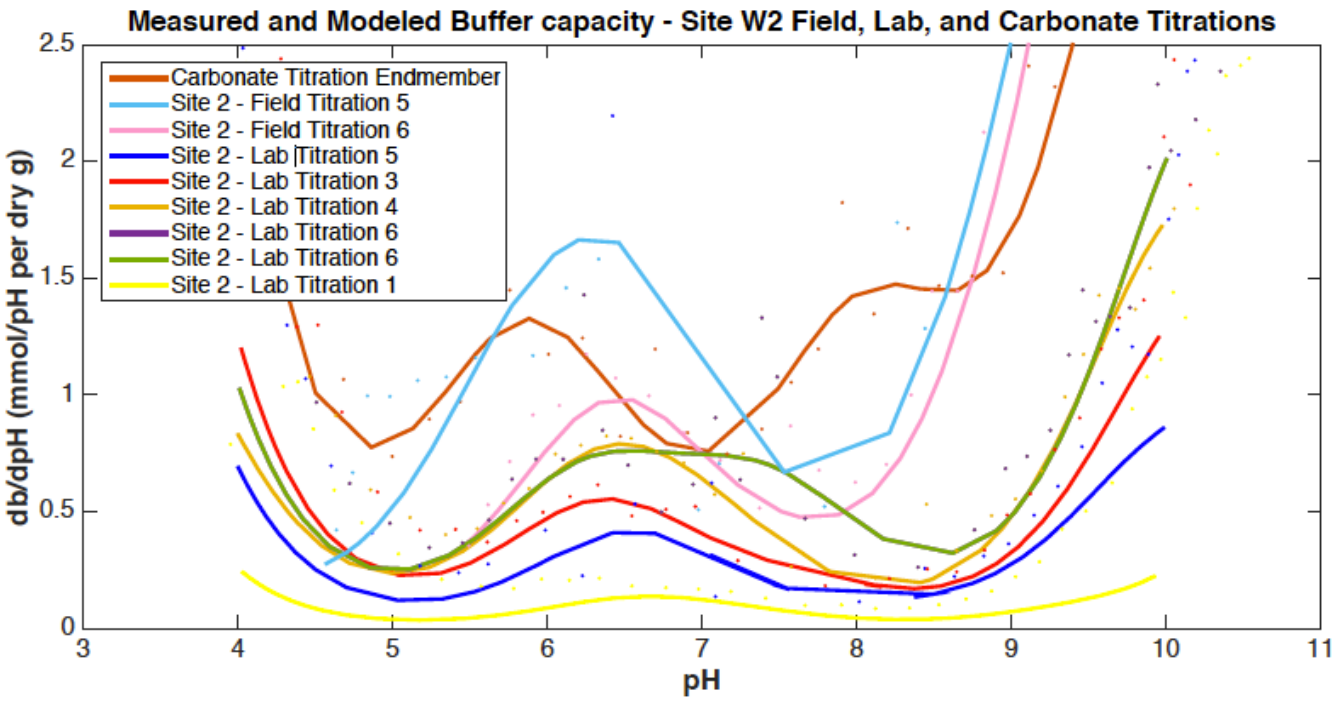

Figure 7. Site W2 modeled buffering capacity for lab and field titrations, as well as a lab end-member titration of the field carbonate.

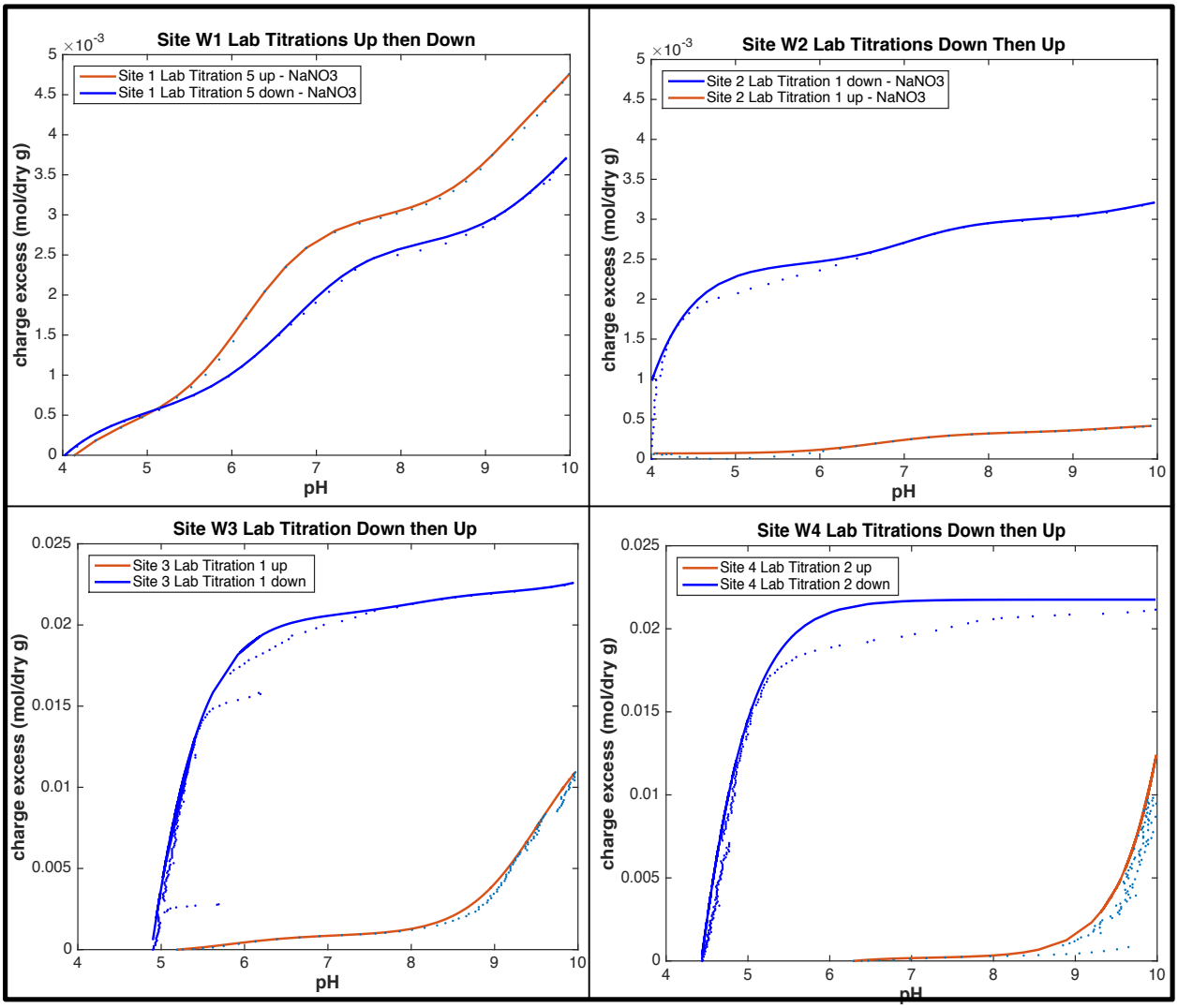

Figure 8. Coupled forward and reverse lab titrations for sites 1-4, showing irreversibility (hysteresis) of titrations due to the presence of authigenic carbonate minerals in the mat samples.

5. Discussion

Our results indicate that the authigenic carbonate mineral fraction of the mat significantly interfered with the titration results, adding complexity to the microbial mats in their natural setting. Carbonates buffer the system and consume protons during the acidic portions of the potentiometric titration process, so that pKa constants for microbial surface ligands cannot be determined. To initiate a potentiometric titration, acid is initially added to decrease the pH to 3, and base is then added incrementally for the up titration. Protons added to adjust the pH to 3 are consumed by the dissolution of $CaCO_{3(s)}$, which pushes the carbonate solution concentration up and generates $CO_{2(g)}$. Even at pH 3, however, carbonate grains are still visible in the analyte

solution. Accordingly, the system never reaches equilibrium prior to the beginning of the up titration, or else all of the carbonate minerals would be consumed by the added acid. The application of titrations to surface reactivity experiments depends on a system at equilibrium. Therefore, the pKa and site concentrations we model in this study are not true values. However, using the titrator to model instantaneous reactivity is reasonable for this study because we are qualitatively (not quantitatively) comparing the relatively surface reactivities of microbial mats in the field and laboratory. Any error induced by non-equilibrium carbonate conditions should be shared by both sets of titrations.

When low pH is finally reached, any remaining carbonate is present as $H_2CO_{3(aq)}$. As pH increases to the 6-8 range, the bulk of the $H_2CO_{3(aq)}$ has deprotonated and become $HCO_3^-{}_{(aq)}$. A similar process occurs at pH 10 when the bulk of the $HCO_3^-{}_{(aq)}$ has deprotonated and become $CO_3^{2-}{}_{(aq)}$. The dissolution of carbonate minerals during the titration is an irreversible process and is likely responsible for the majority of the hysteresis observed here. These results mirror those of Lalonde et al. (2007a,b) where all suspensions of electrolyte-washed mat samples were shown to exchange more protons over the titration range than their acid-washed counterparts.

The deprotonation of $HCO_3^-{}_{(aq)}$ by pH 10 could help explain the large site concentrations modeled for field titrations at sites 3 and 4. The apparent disappearance of these "ligands" after transport to the lab can be explained by a loss of some of the carbonate material during more rigorous lab washing procedures, and an increased attempt at physically removing the carbonate before titrations. The lack of these sites in samples 1 and 2 may be explained by the varying morphology of the mats. Samples 3 and 4 are densely packed and more cohesive microbial mats that could allow for the preservation of carbonate minerals in the interior of the mats. On the other hand, sample 1 is organized in thin strands, while sample 2 is much thinner and gelatinous. A larger portion of their surface area is exposed to the surrounding water making them much less likely to "shield" carbonate minerals from dissolution. Therefore, in the initial step of the potentiometric titration when the pH is brought down below 3, most of the carbonate minerals would have been dissolved and unable to re-precipitate due to the loss of CO_2.

The above inference is reinforced by the buffering capacity curves. All samples appear to show an increase in buffering capacity between pH 9 and 10, coinciding with the release of protons from $HCO_3^-{}_{(aq)}$. Other than this spike, however, these curves show no consistent trend. In theory, W2 shows a buffering capacity signal we may expect if changes in carbonate

concentration dominantly influence buffering capacity. This is most apparent in Figure 7, which shows the titration of a carbonate end-member alongside the site 2 forward-titrations. The sinusoidal shape exhibited by the buffering capacity curve of the carbonate end-member titration is apparent in that of site 2's microbial mat. However, the peaks of the carbonate titration buffering capacity curve appear to be shifted to the left when compared to the site two curves, likely indicating a combined effect of microbial surface ligands and the associated authigenic mineral phase. The amplitude of the carbonate curve is also larger than all site 2 curves, except for field titration 5 and 6. The signal is most closely represented by the carbonate end-member in the case of site 2 due to the mat morphology, as compared to other sites. Site 2 was a thin gelatinous mat composed of diatoms. A large portion of the bottom surface was covered in large carbonate grains that could not be separated from the mat. It is likely that carbonate covered a larger portion of the total surface area of the mat at site 2 compared to the carbonate/surface area ratio of mats at the other sites, thereby accounting for the carbonate dominated buffering in these samples.

EDTA washed samples show a lower buffering capacity than their $NaNO_3$ washed counterparts. This is opposite to what was expected as EDTA typically helps to strip off metals from any previously occupied organic or inorganic ligands. Instead, it is interpreted that EDTA aids in the dissolution of carbonate minerals. The aided dissolution of carbonate minerals by EDTA and the removal of carbonates from the system lowers the overall proton-reactivity of the whole mat sample. Essentially, although the reactivity of the organic component may increase because the metals have been stripped from the surface, there are less carbonate minerals present so the system as a whole is less reactive.

The hysteresis in the forward and reverse coupled titrations suggest we are not dealing with equilibrium conditions. The forward and reverse lab titrations for W1 are much closer to being identical than the other three. This may be an effect of the differing titration protocol. For this example of location W1, an up titration was completed before a down titration. For the other three titrations, a down titration was completed before an up titration. Titration up and then down would have led to the initial dissolution of carbonate minerals as the pH was brought down to ~3 before adding titrant. As this would have released CO_2 from the system, the carbonate minerals would not have reprecipitated during the up titration due to constant flushing of the solution with N_2 gas and the inability of CO_2 to re-enter the system. An alternative explanation could be the

precipitation of $Ca(OH)_{2(s)}$ at high pH. Adjusting the pH to ~11 before titration with acid during the down-up titrations would have instead led to the precipitation of excess calcite and/or $Ca(OH)_{2(s)}$ before its eventual dissolution during the down titration. Again, CO_2 would have escaped and much less excess surface charge would have been measured at each pH because the majority of inorganic carbonate was lost.

Evidence for the deprotonation of carbonate species is best characterized by the sharp increase in excess charge observed between pH 8-8.5 in the majority of the samples, which we will herein refer to as the "carbonate spike" (Figure 4). Only samples W1 and W4 in background electrolyte solution ($NaNO_{3(aq)}$) failed to show a carbonate spike over this range during field titrations. It is apparent that a method for the complete separation of carbonates from microbial mats is required before field titrations in carbonate environments can be successfully applied. However, the titration of mats and their associated carbonates most likely represents a more realistic, although complicated, view of the reactivity of microbial mat surfaces to changes in pH in natural settings.

Assessing the relative contributions of both the authigenic carbonate grains and the organic material to surface reactivity is a necessary next step to assessing the reactivity of complex natural mats. Here we have shown that under field conditions, numerous variables are present that cannot be accounted for by laboratory titrations alone. This study also highlights the need for an investigation into the effect of mat morphology on the kinetics of proton uptake, as potentiometric titrations assume equilibrium is reached after each acid or base addition. While potentiometric field titrations may be useful in silica-rich mat systems (e.g., hot spring sinters, siliciclastic sediments), in carbonate-rich systems the reaction of protons with authigenic carbonate phases inhibits the determination of biomass equilibrium constants (pKa) and site concentrations. Despite this limitation, we show here that the in-situ reactivity of microbial mats varies greatly from identical samples titrated in a laboratory days later. This finding has significant implications for future surface complexation modelling and its use in developing accurate quantitative metal adsorption values for metals remediation work in natural environments.

6. Conclusion

Although the potential benefit of conducting potentiometric titration experiments in the field is significant, the procedure requires streamlining and adjustments to account for factors not typical of laboratory experiments, such as the presence of authigenic carbonate precipitates. In the case of hot springs and potentially in many natural systems, carbonates yield a "carbonate spike" in the titration data introduced by the contribution of inorganic carbonate mineral dissolution and subsequent carbonate speciation changes during the transition from low to high pH, consistent with the interpretation of Lalonde et al. (2007a,b). This inhibits the determination of microbial surface ligand variety and concentrations. Determination of the reactivity of the mat biomass could be achieved by physically removing larger grains of authigenic carbonates, and repeatedly treating the biomass with weak acid washes until remaining carbonate solids are removed. The resulting biomass could be titrated to quantify pKa and surface functional group concentrations. Mat carbonates can be separated from the organic material using a hexane-water technique, and their reactivity assessed as described here (Figure 7). Finally, determining the role of metal sorption to biomass versus incorporation in, or sorption to, authigenic carbonate minerals in the mats would shed light on the primary trace metal immobilization mechanisms in hot springs. This study clearly demonstrates that the determination of surface reactivity in the field is much more complex than traditional laboratory based experiments. The implications of using laboratory generated data in generating surface complexation and metal adsorption models for natural systems merits further investigation.

Acknowledgements

Funding from NSERC to D.S.A. and K.O.K supported this work.

6.References

-Alessi, D.S., Fein, J.B., 2010. Cadmium adsorption to mixtures of soil components: Testing the component additivity approach. Chemical Geology 270 (1), 186-195.

-Bethke, C.M., Brady, P.V., 2000. How the K_d approach undermines ground water cleanup. Ground Water 38 (3), 435-443.

-Borrok, D., Fein, J.B., Kulpa, C.F., 2004a. Proton and Cd adsorption onto natural bacterial consortia: testing universal adsorption behavior. Geochimica et Cosmochimica Acta 68 (15), 3231-3238.

-Borrok, D.M., Fein, J.B., Kulpa Jr., C.F., 2004b. Cd and proton adsorption onto bacterial consortia grown from industrial wastes and contaminated geologic settings.

-Clague, J.J., 1975. Late Quaternary sediments and geomorphic history of the southern Rocky Mountain Trench, British Columbia. Can. J. Earth Sci. 12, 595-605.
-Daughney, C.J., Fowle, D.A., Fortin, D., 2001. The effect of growth phase on proton and metal adsorption by *Bacillus subtilis*. Geochimica et Cosmochimica Acta 65 (7), 1025-1035.
-Davis, J.A., Coston, J.A., Kent, D.B., Fuller, C.C., 1998. Application of the surface complexation concept to complex mineral assemblages. Environmental Science and Technology 32, 2820-2828.
-Fein, J.B., Daughney, C.J., Yee, N., Davis, T.A., 1997. A chemical equilibrium model for metal adsorption onto bacterial surfaces. Geochimica et Cosmochimica Acta 61 (16), 3319-3328.
-Fein, J.B., Martin, A.M., Wightman, P.G., 2001. Metal adsorption onto bacterial surfaces: Development of a predictive approach. Geochimica et Cosmochimica Acta 65 (23), 4267-4273.
-Fowle, D.A., Fein, J.B., 1999. Competitive adsorption of metal cations onto two gram positive bacteria: Testing the chemical equilibrium model. Geochimica et Cosmochimica Acta 63 (19/20), 3059-3067.
-Fowle, D.A., Fein, J.B., 2000. Experimental measurements of the reversibility of metal-bacteria adsorption reactions. Chemical Geology 168, 27-36.
-Grasby, S.E., and Hutcheon, I., 2001. Controls on the distribution of thermal springs in the southern Canadian Cordillera. Can. J. Earth Sci. 38:427-440.
-Herbelin, A.L., and Westall, J.C., 1999. FITEQL 4.0: A computer program for determination of chemical equilibrium constants from experimental data. Department of Chemistry, Oregon State University.
-Koretsky, C., 2000. The significance of surface complexation reactions in hydrologic systems: a geochemist's perspective. Journal of Hydrology 230, 127-171.
-Lalonde, S.V., Amskold, L.A., Warren, L.A., Konhauser, K.O., 2007a. Surface chemical reactivity and metal adsorptive properties of natural cyanobacterial mats from an alkaline hydrothermal spring, Yellowstone National Park. Chemical Geology 243, 36-52.
-Lalonde, S.V., Amskold, L., McDermott, T.R., Inskeep, W.P., Konhauser, K.O., 2007b. Chemical reactivity of microbe and mineral surfaces in hydrous ferric oxide depositing hydrothermal springs. Geobiology 5, 219-234.
-Lalonde, S.V., Smith D.S., Owttrim, G.W., Konhauser, K.O., 2008a. Acid-base properties of cyanobacterial surfaces 1: influences of growth phase and nitrogen metabolism on cell surface reactivity. Geochimica et Cosmochimica Acta 72, 1257-1268.
-Lalonde, S.V., Smith, D.S., Owttrim, G.W., Konhauser, K.O, 2008b. Acid-base properties of cyanobacterial surfaces. II: silica as a chemical stressor influencing cell surface reactivity. Geochimica et Cosmochimica Acta 72, 1269-1280.
-Lalonde, S.V., Dafoe, L.T., Pemberton, S.G., Gingras, M.K., Konhauser, K.O., 2010. Investigating the geochemical impact of burrowing animals: Proton and cadmium adsorption onto the mucus lining of *Terebellid* polychaete worms. Chemical Geology 271, 44-51.
-Lovley, D.R., Coates, J.D., 1997. Bioremediation of metal contamination. Current Opinion in Biotechnology 8, 285-289.
-Malik, A., 2004. Metal bioremediation through growing cells. Environment International 30, 261-278.
-Martinez, R.E., Smith, D.S., Kulczycki, E., Ferris, F.G., 2002. Determination of intrinsic bacterial surface acidity constants using a Donnan shell model and a continuous pK_a distribution method. J. of Colloid and Interface Science 253, 130-139.

-Phoenix, V.R., Martinez, R.E., Konhauser, K.O., Ferris, F.G., 2002. Characterization and implications of the cell surface reactivity of *Calothrix* sp. strain KC97. Applied and Environmental Microbiology 68 (10), 4827-4834.
-Pickering, B., 1954. Principal hot springs of the southern rocky mountains of Canada. Guide Book Fourth Annual Field Conference Banff-Golden-Radium, 146-148.
-Rainey, D.K., Jones, B., 2009. Abiotic versus biotic controls on the development of the Fairmont Hot Springs carbonate deposit, British Columbia, Canada. Sedimentology 56, 1832-1857.
-Van Everdingen, R.O., 1972. Thermal and mineral springs in the southern Rocky Mountains of Canada. Water Management Service, Department of the Environment, Ottawa, ON. 151 pp.
-Worldweatheronline.com,. 'World Weather Online | World Weather | Weather Forecast'. N.p., 2015. Web. 30 Nov. 2015.
-Yee, N., and Fein, J.B.,, 2003. Quantifying metal adsorption onto bacteria mixtures: A test and application of the surface complexation model. Geomicrobiology Journal 20 (1), 43-60.